

Pathways and Kinetics of Anisole Pyrolysis Studied by NMR and Selective ^{13}C Labeling. Heterolytic Carbon Monoxide Generation

Yasuo Tsujino, Yoshiro Yasaka,† Nobuyuki Matubayasi, and Masaru Nakahara*

Institute for Chemical Research, Kyoto University, Uji, Kyoto 611-0011

Received October 31, 2011; E-mail: nakahara@scl.kyoto-u.ac.jp

By applying ^{13}C and ^{1}H NMR spectroscopy the pyrolysis of site-selectively ^{13}C-enriched ($H_3{}^{13}CO{}^{12}C_6H_5$) and normal anisole compounds was studied in the dark at 0.001–1.0 M (M, mol dm^{-3}) and at 400–600 °C (supercritical conditions). Conversion of the ^{13}C-labeled methyl group was confined to the methoxy-originated fragments, ^{13}CO and $^{13}CH_4$, and the reactive intermediate, $H^{13}CHO^*$. The normal phenyl group, $^{12}C_6H_5$– was converted to benzene, $^{12}C_6H_6$ and phenol, $^{12}C_6H_5OH$ without ring disintegration. The pyrolysis consists of two elementary steps: (1) the rate-determining unimolecular ether-bond fission (k_1) to generate the fragmented product C_6H_6 and energized intermediate $H^{13}CHO^*$ through the intramolecular proton transfer from the methoxy group to the phenyl, and (2) the fast bimolecular disproportionation (k_2) through the intermolecular proton/hydride transfer from $H^{13}CHO^*$ to $H_3{}^{13}COC_6H_5$ to produce ^{13}CO, $^{13}CH_4$, and C_6H_5OH. CO is generation by the heterolytic (ionic) mechanism in contrast to the homolytic (radical) one via the phenoxy radical intermediate ($C_6H_5O\bullet$) in the literature despite the agreement of the rate constant (k_1) and the activation energy.

It is important to investigate the kinetics and mechanisms of the thermal reaction process of ethers in order to understand more deeply high-temperature reactions and to develop more efficient high-temperature cracking and processing of fossil (oil and coal) and biomass fuels. In the previous letter,[1] we reported a kinetic study on the noncatalytic pyrolysis of the asymmetric ether, anisole (methyl phenyl ether), at 1 M and at 400–430 °C. By the product analysis with the gas- and liquid-phase NMR we have succeeded in revealing that the thermal fragmentation of the ether is induced by not homolytic (radical) but heterolytic (ionic) C–H bond fission, and that the reaction consists of the slow and the fast elementary steps: (1) The slow step is the unimolecular C–H bond fission that is initiated by the intramolecular proton transfer from the methyl to the phenyl group to generate the reactive intermediate formaldehyde (HCHO*). (2) The fast step is composed of the successive intermolecular proton and hydride transfers over the electronegative oxygen atom from the thermally excited intermediate HCHO*, respectively, to the phenoxy and methyl groups of the parent anisole molecule. They are expressed as:

$$C_6H_5OCH_3 \rightarrow C_6H_6 + HCHO^* \text{ (slow)} \quad (1)$$

$$C_6H_5OCH_3 + HCHO^* \rightarrow C_6H_5OH + CH_4 + CO \text{ (fast)} \quad (2)$$

As represented here, the major products of the high-pressure (concentration) pyrolysis are benzene, phenol, methane, and carbon monoxide, all in almost equal amounts. The intramolecular proton transfer induced by the C–O–C bending mode was also observed for acetaldehyde,[2] and dimethyl and diethyl ethers; This is called "hinge reaction" at high temperature.[3,4] When the elementary steps assumed previously (see below) were the case, CO carbon should come from the methoxy but not from the phenoxy. To test this, here we have selectively labeled the asymmetric ether, anisole, by ^{13}C as C_6H_5–O–$^{13}CH_3$.

In all of the earlier papers,[5–12] the following radical CO pathway was postulated:

$$C_6H_5OCH_3 \rightarrow C_6H_5O\bullet + CH_3\bullet \quad (3)$$

$$C_6H_5O\bullet \rightarrow C_5H_5\bullet + CO \quad (4)$$

The homolytic bond breakage is assumed to take place between the ether oxygen (eq 3) and the methyl carbon to generate the methyl and phenoxy radicals, and furthermore, the ring-size reduction is presumed to give rise to CO as in eq 4. The thermal fragmentation of dimethyl ether, which is regarded as the prototype of the "unimolecular reaction," has been believed to have the radical mechanism since the pioneering work by Hinshelwood and co-workers in the 1920s.[13] The methoxy group is a key characteristic of these symmetric and asymmetric ethers, and the reactive intermediate formaldehyde* is expected to be generated for both cases. The asymmetric ether can be a promising candidate to distinguish the reaction pathways for the generated hydrocarbon fragments: benzene and methane for anisole and only methane twins for dimethyl ether. Convincing evidence is wanted to resolve the discrepancy in the mechanism of the fundamental thermal reaction. To this end we have scrutinized the CO generation pathway by applying high-resolution NMR spectroscopy to the labeled anisole studied in the dark to carefully avoid the interference by photochemical radical processes. In this work the quantitative overall product analysis with the mass balance strictly confirmed by NMR is carried out to demonstrate that the reaction mechanism is correctly represented by the elementary steps given by eqs 1 and 2.

† Present address: Institute for Computational Molecular Science, Temple University, Philadelphia, Pennsylvania 19122-6078, USA

Published on the web December 30, 2011; doi:10.1246/bcsj.20110334

Our[1] and the other[6–12] investigations focus on the pyrolysis, respectively, at high (1.0 M) and low (0.1–10 mM) concentrations (pressures). In these works some products are common but others are different probably due to differences in method for product analysis. Here we show that the mechanistic discrepancy does not come from differences in the reaction conditions, such as the concentration and the temperature. We have scrutinized in detail the rate laws and kinetics for supercritical anisole reaction by covering wide enough ranges of concentrations and temperatures. Analytical connectivity of the kinetics between the high- and low-concentration limits has been also demonstrated. The anisole depletion rate constants in this work and those in the literature[6–9] are in good agreement, showing the same Arrhenius relation over the wide temperature range of 400–700 °C. Thus the unimolecular bond fission mechanism is the same at the low and high pressures, see eq 1.

In the following section, the experimental features are described. In the third section, the NMR spectroscopic results are analyzed quantitatively as much as possible to discuss the pyrolysis mechanism. Conclusions are given in the last section.

Experimental

The labeled anisole ($H_3{}^{13}COC_6H_5$, purity >99%) was synthesized from phenol (Nacalai; purity >99%) and ^{13}C-enriched iodomethane (ISOTEC; purity >99%) by the Williamson synthesis.[14] The deuterated solvents, benzene-d_6 and toluene-d_5 were supplied by ISOTEC. Anisole was loaded into a quartz tube of 1.5-mm i.d. and 3.0-mm o.d, and 150-mm height to set the desired concentration (1.0 M) in the homogeneous gas phase at 400–600 °C; for example, the liquid reactant was 20 mm high at room temperature for the supercritical reaction of anisole at 1.0 M, and the pressure of the sample gasified at 500 °C corresponds to 6.3 MPa according to the ideal-gas law before pyrolysis. For the reaction at a low concentration of 1.0 mM a high-precision pyrex NMR tube (Shigemi Co., Ltd.) with a diameter of 5 or 10 mm was employed. Oxygen dissolved and/or adsorbed in the sealed sample was completely removed by argon gas. In order to avoid photochemical processes, the sample was put into a steel pipe kept in advance at a desired temperature in a programmable electric furnace; the temperature was controlled within ±1 °C. Without opening the sample tube, the quenched gas and liquid phases were subjected to quantitative ^{13}C and ^{1}H NMR measurements at room temperature using ECA400 (JEOL) and 600-MHz spectrometer (ECA, JEOL). ^{13}C NMR signals in the gas phase were collected with sufficient delay times without proton irradiation in order to quantify the concentrations of the reactant and products. At high temperatures (>500 °C) a number of reactor tubes were simultaneously put into the furnace and taken out as a function of reaction time. To make a correction for the effect of the dead time required for the heating of the tube the early time portion (≈1 min) was cut from all of the kinetic data.[15] The sample setup and relevant techniques for NMR measurements in the liquid and the gas phases have been described elsewhere.[1–4] Yields for the reactant and products were obtained from the peak intensity within an error of a few percent.

Results and Discussion

We elucidate reaction pathways and mechanisms by monitoring all of the intermediate and final products of ^{13}C-labeled and normal anisole reactants. High-resolution ^{1}H and ^{13}C NMR spectra taken in both the gas and the liquid phases are used extensively for the elemental and structural analyses under the H and C mass balances. To confirm the newly found heterolytic proton-transferred mechanism we carry out a comprehensive kinetic analysis. We show that the nonradical mechanism operates not only at high but also at low concentrations over a wide temperature range.

Product Distribution and Reaction Pathways. Figure 1 shows the ^{1}H and ^{13}C NMR spectra taken at room temperature for the study on the thermal fragmentation of anisole in the supercritical condition at 500 °C.[16] In panel a, there is given the ^{13}C spectrum of the reactant C_6H_5–O–$^{13}CH_3$. Only one strong peak is observed in the high magnetic field. This is assigned to the enriched methyl carbon; in fact, the signal is a quartet due to the spin coupling of the ^{13}C with the three methyl ^{1}H's. Only when the intensity axis is expanded (not shown here) the naturally abundant phenyl carbons are observable reflecting the low ratio of ^{13}C (≈1%); the relative intensity of each phenyl carbon was determined to be (0.98 ± 0.02)% according to ^{13}C NMR analysis in high precision. Correspondingly the isotope side-bands were observed as weak ones in the ^{1}H spectra, which are rather complicated by the fine structures of various ring-proton signals. The ^{13}C enrichment is so selective and extensive (>99%) that we can unambiguously discuss the CO reaction pathway.

First we discuss which products are in the liquid phase in the NMR measurement of the reaction system quenched to room temperature. Of the four major products, benzene, phenol, methane, and carbon monoxide, the ring compounds, benzene and phenol, exist in the liquid phase at room temperature as well as the reactant anisole. These ring compounds collectively serve as liquid "solvent" in the sealed quartz tube reactor of 150-mm height for the other gaseous products, CO and CH_4. In the reaction system these small nonpolar molecules quenched are partitioned between the gas and the liquid phases depending on the solubility or Henry's constant. The CO partition ratio of the gas to the liquid phases is high as mentioned below in the closed system where the volume ratio of the gas to the liquid phases is ≈13/2; the liquid volume slightly increases with the fragmentation reaction time at most by 10%. To scrutinize the CO pathway in a reliable manner we should pay attention to the spectrum in the gas phase rather than that in the liquid phase.

In panel b we see the methyl carbon destinations at the reaction time of 20 min where the pyrolysis is almost completed (yield > 95%). It turns out that the end products are ^{13}CO and $^{13}CH_4$. The former and the latter are given, respectively, by the oxidation and the reduction of the methoxy group. We can conclude that the CO comes from the methoxy in harmony with the scheme given by eqs 1 and 2. The prevailing phenoxy radical mechanism given by eqs 3 and 4 is not supported by the present investigation.

The peak intensity of ^{13}CO in panel b is slightly larger than that of $^{13}CH_4$ because the solubility of ^{13}CO is lower than that of $^{13}CH_4$ in the liquid "solvent;" see the ^{13}C spectrum in

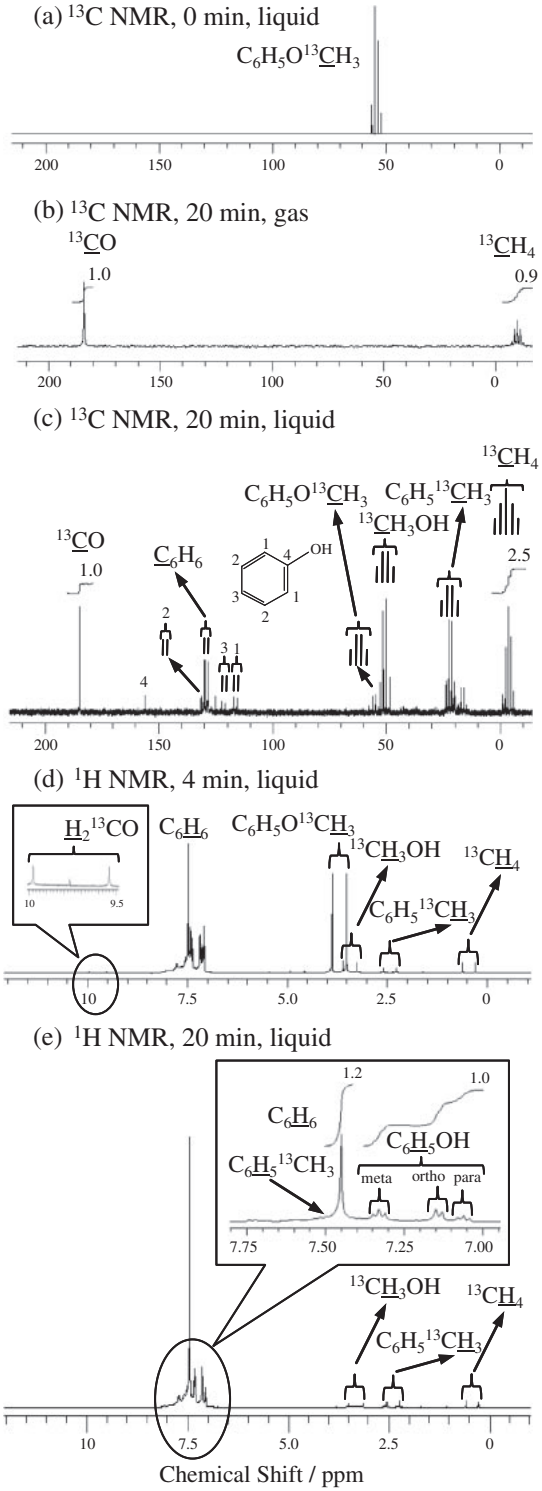

Figure 1. ^{13}C and ^{1}H NMR spectra for the reactant and products of labeled anisole treated at 500 °C. (a) ^{13}C spectrum before reaction, (b) gas ^{13}C spectrum after 20 min, (c) liquid ^{13}C spectrum after 20 min, (d) liquid ^{1}H spectrum after 4 min, and (e) liquid ^{1}H spectrum after 20 min. In panels (b) and (c), the numerical value above the curve indicates the integrated intensity for each peak. The weak peak at 3.2 ppm was assigned to water.

panel c. When the signal intensities of the species in panel b are compared with those in panel c, the partition mole ratios are determined to be 20(gas)/1(liquid) for ^{13}CO and 10(gas)/1(liquid) for $^{13}CH_4$ in the present volume ratio of the gas to the liquid phase (13/2). In panel c the ^{13}C signal intensities of benzene and phenol are quite low as a consequence of the natural abundance ($0.98\% \pm 0.02\%$ by NMR), and the intensities are coincidentally comparable with those of sparingly soluble ^{13}CO or $^{13}CH_4$. In any event, the ring carbons of benzene and phenol keep the natural abundance of ^{13}C without any scrambling by the enriched methyl carbon (^{13}C) in anisole. Thus the phenyl ring of anisole is not disintegrated during the reaction course, in disagreement with eq 4.

The heterolytic CO pathway, not from the phenoxy but from the "methoxy" as described mechanistically in Figure 2, can be confirmed by using the ^{1}H spectra in panels d and e at intermediate and almost final reaction times, respectively. The ring products, benzene and phenol, are "equally" generated as in the case of the methyl-originated products, methane and carbon monoxide; note the integrated ^{1}H signal intensity ratio of benzene to phenol that is not 1 but $6/5 = 1.2$ as shown in the expanded chart between 7.00 to 7.50 ppm in panel e, just corresponding to the ratio of the ring protons. The essential counterpart of the CO pathway from the methoxy is the retention of the phenyl ring during the proton-transferred ether bond fission. In fact, the total number of ring protons contributed from benzene (eq 1) and phenol (eq 2) does not decrease but increases as shown by the time-dependent ^{1}H mass balance in Figure 3. The increase is the evidence for the proton transfer from the methyl to the phenyl to produce benzene through eq 1, which results in the increase in the number of the ring ^{1}H's from 5 to 6 with the total ^{1}H mass balanced before and after the reaction (Figure 3). After the proton transfer, there is generated ^{13}C-labeled formaldehyde whose proton is actually observed as the doublet peak (see panel d). Energized formaldehyde*, which is conjectured to be vibronically excited by the excess energy generated by the bond dissociation, is originated as a reactive intermediate from the enriched methoxy through the intramolecular proton transfer.[17] The thermal decomposition of anisole consists of the bond breakage induced by the intramolecular proton-transfer step (eq 1) and the intermolecular proton and hydride transfer step (eq 2) as pictorially summarized in Figure 2.

Intra- and intermolecular proton-transfer mechanisms proposed above are justified in view of the charge distribution in anisole. The phenyl ring and the oxygen atom in anisole have a negative partial charge, respectively, due to the π and the lone-pair electrons, and the hydrogen atom of the methyl group has a weakly positive charge ($\approx 0.1e$). Hence the methyl hydrogen can slide on the oxygen atom surface as a *proton* from the methyl site to the phenyl surface without leaving the molecular surface. The proton migration can be driven by the thermal excitation of the internal vibration and/or rotation modes. In eq 2 the proton migration is followed by the hydride transfer from the state negatively charged by the proton leaving as the first step (Figure 2).

Mass Balances and Mechanisms. Figure 3 shows the plots of mass balances for the elements ^{1}H and ^{13}C and conversion fractions of the four major products and the reactive

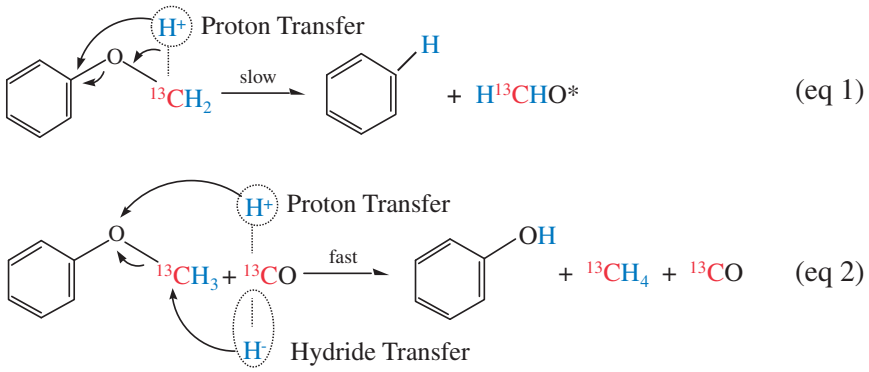

Figure 2. Reaction scheme for anisole pyrolysis.

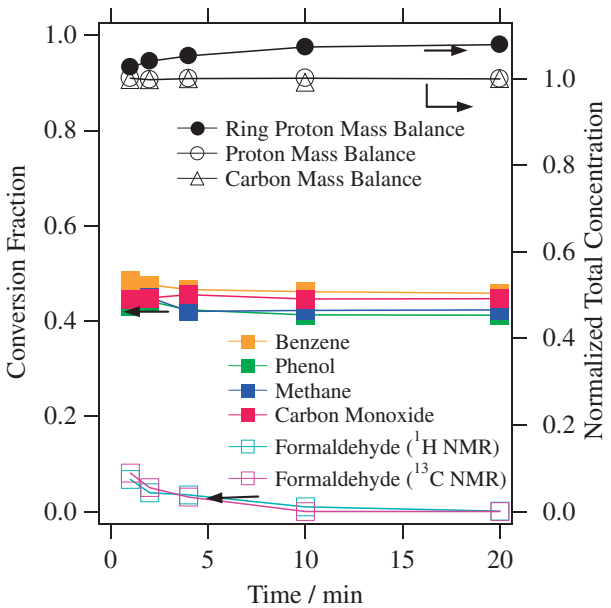

Figure 3. Time dependencies of conversion fractions for the four major products and formaldehyde intermediate, and those of the ^{1}H and ^{13}C total mass balances together with the ring ^{1}H mass balance at 500 °C.

intermediate against the reaction time. The conversion fraction f is defined by the product yield (Δ[product]) normalized by the amount of anisole (-2Δ[anisole]) consumed by the two pyrolysis steps given by eqs 1 and 2; $f = -\Delta[\text{product}]/2\Delta[\text{anisole}]$. The comprehensive analysis of the products in both the gas and liquid phases enables us to examine in more detail reaction pathways; in Figure 3 note the ^{1}H and ^{13}C mass balances maintained in a high degree at each reaction time. An ideal reference value of f for the major products is obtained by adding eqs 1 and 2 to have the following overall reaction:

$$2\,{}^{12}C_6H_5O{}^{13}CH_3 \rightarrow {}^{12}C_6H_6 + {}^{12}C_6H_5OH + {}^{13}CH_4 + {}^{13}CO \quad (5)$$

Here the intermediate and by-products are dropped out, and the bimolecular conversion (stoichiometric) fraction defined above takes the ideal value, 1/2.

The deviation of the conversion fraction from the ideal is a measure for the competition extent (weight) of the side-

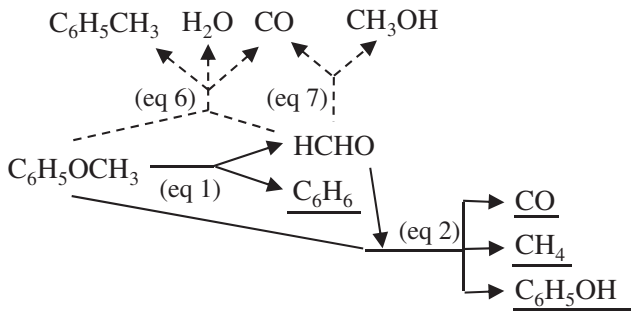

Figure 4. Reaction pathways of anisole pyrolysis. Solid-line arrows represent main pathways and broken lines the minor. Main products are underlined. For the explanation see the text.

reactions generating toluene and methanol. As seen in Figure 3, each conversion fraction is slightly less than the ideal value (1/2), as a result of the conversion of the reactive intermediate, formaldehyde*, into the other by-products in addition to one of the major products, phenol. These reaction pathways for the prototypical pyrolysis are summarized in Figure 4.[18] Let us discuss slight deviations from the above-mentioned reference value (1/2) in terms of the side-reactions. Toluene can be formed by

$$\begin{aligned} &{}^{12}C_6H_5O{}^{13}CH_3 + H{}^{13}CHO^* \\ &\quad \rightarrow {}^{12}C_6H_5{}^{13}CH_3 + H{}^{13}COOH \\ &\quad \rightarrow {}^{12}C_6H_5{}^{13}CH_3 + {}^{13}CO + H_2O \end{aligned} \quad (6)$$

where the migration of the methyl cation (not radical) is assumed. Methanol can be produced by the following self-disproportionation reaction[15] of formaldehyde* via the proton and hydride transfers:

$$2H{}^{13}CHO^* \rightarrow {}^{13}CH_3OH + {}^{13}CO \quad (7)$$

The conversion fraction of the intermediate formaldehyde* is consumed more by these side-reactions. The conversion fractions (parenthesized numbers) of the major products (underlined below), the by-products, and the intermediate at 1 min (early reaction stage) are in the following sequence:

$$\begin{aligned} &\underline{\text{benzene } (0.48_5)} > \underline{\text{CO } (0.45)} > \underline{\text{methane } (0.44)} \\ &\quad \approx \underline{\text{phenol } (0.43)} > \text{formaldehyde}^* \ (0.04) > \text{toluene } (0.01_5) \\ &\quad \approx H_2O \ (0.01_5) > \text{methanol } (0.00_5) \end{aligned} \quad (8)$$

Now we can confirm the competition of the side-reactions consuming the intermediate formaldehyde* as shown in Figure 4 by checking the following mass balance:

$$f(\underline{\text{benzene}}) = f(\text{formaldehyde}^*) + [f(\underline{\text{phenol}}) + f(\text{toluene}) + 2f(\text{methanol})] \quad (9)$$

On the right-hand side of eq 9 the 1st term is the remained intermediate and the bracketed terms are corresponding to the consumed one (Figure 4). The sum value for the right-hand side at the early reaction stage is equal to 0.48_9, which is very close to the conversion fraction for benzene (0.48_5). A small amount of deviation (0.01_1) of the conversion fraction of benzene from the ideal is approximately equal to the value for toluene (0.01_5), which corresponds to the branched conversion of anisole to toluene as can be seen from the reaction pathways summarized in Figure 4. At the almost final reaction stage (20 min) the sum value for the right-hand side of eq 9 is equal to 0.47, which is very close to the conversion fraction for benzene (0.46). The slightly increased deviation (0.03) of the conversion fraction of benzene from the ideal is equal to the value for toluene (0.03) as in the case of the early reaction stage. For the same reason the conversion fraction for benzene is the largest as seen in Figure 3.[19] The product distribution is neither broadened nor flattened at all, in contrast to the radical mechanism where the branching and propagation take place after a long reaction run. Thus the quantitative overall product analysis based on the NMR elemental and structural analysis is in harmony with the reaction pathways established in Figure 4.

Now let us compare the products identified here with those in the literature.[5–12] The four major products we identified and quantified are ring-containing phenol and benzene, and the counter products, carbon monoxide and methane. A full set of these products were reported along with some other ring compounds in several papers.[1,7,9,11] The presence of phenol as one of the ring products, which is a clear indication of the retention of the C–O bond between the phenyl carbon and the oxygen, was reported in *all* of the papers[1,6–12] except for an MS (mass spectroscopy) study of anisole pyrolysis.[5] This earliest work at a very high temperature of 950 °C referred to the *possibility* of formation and decomposition of phenoxy to carbon monoxide. The key product, carbon monoxide was actually reported in *all* of the papers[1,5–12] at the lower temperatures of 400–600 °C.[1,6–9,12] Methane was found in *most* of the papers.[1,6,7,9,11,12] In *several* papers,[1,7,9–11] benzene was found as the ring product, always accompanied by phenol and carbon monoxide. All of the information on the product distribution implies the *phenyl ring retention* and is not contradictory to the bimolecular proton-transfer step (eq 2) followed by the unimolecular proton-transfer step (eq 1). Thus the present results on the products qualitatively agree with those previously reported despite the difference in the proposed mechanism.

Such traditional methods as GC (gas chromatography) and MS for the product analysis lack the power to differentiate molecular structures compared with NMR; GC relies upon the retention-time identity, and MS invasively destroys the molecular structure because of the use of photons or electrons to fragment original molecules into ionized species. One of the major points in this work is to discern the reaction mechanism on the basis of the elemental and structural analysis by NMR (Figure 3). In contrast, the necessary checking of the mass balance was not done in previous reports.[5–12] Reaction mechanism is subject to changes depending on new information on products and intermediate so that the kinetic self-consistency can be maintained. It is indispensable to show that the new proton-transferred mechanism is not specific to the high concentration of 1.0 M at 500 °C. In the following section we proceed to a detailed kinetic analysis of the time evolution of the chemical species involved in order to scrutinize whether a new reaction channel is opened or not in low concentrations so far studied in the literature.

Kinetic Analysis. The reaction pathways in Figure 4 lead us to the rate laws expressed by the following differential equation:

$$\frac{\mathrm{d}[\mathrm{A}]}{\mathrm{d}t} = -k_1[\mathrm{A}] - k_2[\mathrm{A}][\mathrm{F}^*] \quad (10)$$

where t is the time, k_1 and k_2 are the rate constants for the elementary steps given by eqs 1 and 2, respectively, and the symbols [A] and [F*] denote the concentrations of the reactant anisole and intermediate formaldehyde*, respectively. The first term on the right-hand side of eq 10 presents the unimolecular step induced by the intramolecular proton transfer from the methyl group to generate benzene and active intermediate formaldehyde. The second term presents the successive bimolecular step induced by the intermolecular proton transfer from the intermediate F* to the reactant A to give such products as phenol, methane, and carbon monoxide.

Given a functional relationship between [F*] and [A], eq 10 can be integrated. As already noted in Figure 3 [F*] is not constant but somehow related to [A], finally dropping to zero. In Figure 5 it is shown how [F*] depends on [A] at 400 and 500 °C in the neat and carrier or solvent gases added in excess. Benzene is one of the main products and toluene is alien. The ring protons of benzene and toluene are fully deuterated in order to distinguish products of anisole from those of the supercritical solvation shell.[20,21] It turns out that [F*] is linearly related to [A] at both temperatures, and that the linear region is separated into the high (HC) and the low (LC) concentration (pressure) regions; the crossover occurs, respectively, at [A] = ca. 650 and ca. 250 mM at 400 and 500 °C in the supercritical conditions.[16] As the temperature rises [F*] significantly increases as a result of the acceleration of the slow unimolecular ether-bond fission on the phenyl side (eq 1), and in consequence, the crossover concentration decreases with increasing temperature. Although supercritical benzene-d_6 has a negligibly small effect, supercritical toluene-d_5, which is composed of the phenyl and methyl moieties common to anisole, lowers the crossover point.[22] The relation in the HC region is expressed as:

$$[\mathrm{F}^*]^{\mathrm{HC}} = \alpha^{\mathrm{HC}}[\mathrm{A}]^{\mathrm{HC}} + \beta^{\mathrm{HC}} \quad (11)$$

where α^{HC} and β^{HC} are the constant parameters. In the LC region the relation is just proportional with a much larger slope:

$$[\mathrm{F}^*]^{\mathrm{LC}} = \alpha^{\mathrm{LC}}[\mathrm{A}]^{\mathrm{LC}} \quad (12)$$

The linear parameters used for the integration are summarized in Table 1.

Given the linear relation between [F*] and [A], we can reduce the number of the variables in eq 10 and the general solution is obtained separately in the HC and LC regions:

$$\frac{d[A]}{dt} = -(k_1 + \beta k_2)[A] - \alpha k_2[A]^2 \quad (13)$$

$$[A]^{HC} = \frac{(k_1 + \beta^{HC}k_2)[A]_0 \exp[-(k_1 + \beta^{HC}k_2)t]}{k_1 + \beta^{HC}k_2 + \alpha^{HC}k_2[A]_0(1 - \exp[-(k_1 + \beta^{HC}k_2)t])} \quad \text{(HC)} \quad (14)$$

$$[A]^{LC} = \frac{k_1[A]_0 \exp(-k_1 t)}{k_1 + \alpha^{LC}k_2[A]_0[1 - \exp(-k_1 t)]} \quad \text{(LC)} \quad (15)$$

The conventional steady-state approximation corresponds to the limiting case, $\alpha^{HC} = 0$ with β unknown. When an intermediate is observed as in the present case an average intercept, β^{HCA}, may be taken. The rate of the reactant depletion due to the steady-state approximation is combined to the present linear-relation approach. For the intermediate F* the rate law is:

$$\frac{d[F^*]}{dt} = k_1[A] - k_2[A][F^*] \quad (16)$$

In the steady-state approximation $d[F^*]/dt = 0$ and $[F^*] = \beta^{HCA}$ are assumed. Hence it follows that

$$k_2 = k_1/\beta^{HCA} \text{ (HC)} \quad (17)$$

By inserting eq 17 into eq 10 we have the limiting expression for $[A]^{HCSS}$ under the steady-state condition:

$$[A]^{HCSS} = [A]_0 \exp(-2k_1 t) \text{ (HCSS)} \quad (18)$$

The apparent depletion constant in the HCSS condition is double the rate constant for the slow unimolecular step (eq 1) due to the assumption for the extremely rapid bimolecular step (eq 2). When the intermediate is accumulated up to the critical concentration β^{HCA} the reactant begins to be quickly consumed, and the depletion rate appears to be in the 1st-order with the rate constant two times faster than that of the intrinsically unimolecular step (the first term on the right-hand side of eq 10). The HCSS values of k_1 and k_2 can be obtained respectively from eqs 18 and 17. Surprisingly, the difference in the determined rate constant k_1 between eqs 14 and 18 is confirmed to be negligibly small simply because of the small slope of eq 11.

It is to be noticed that the low anisole concentration, $[A]^{LC}$, can be set initially or approached inevitably at the late stage of the reaction. In the LC limit eq 15 can be switched to:

$$[A]^{LC} = [A]_0 \exp(-k_1 t) \text{ (LC)} \quad (19)$$

The corresponding rate law is obtained from eq 13 as follows: the $[A]^2$ term much (exponentially) smaller than the [A] term is dropped away from the right-hand side where $\beta = 0$. Thus the depletion rate slows down in the LC limit compared to eq 18 because the much faster bimolecular step (k_2, eq 2) disappears. This is ascribed to the dramatic reduction of the encounter probability (density multiplication) of dilute A and F* to form a reactive complex between them in the supercritical conditions.[21] Probably F* is deactivated too much nearer to the ground state in a long mean-free-path.[22–24] In this LC limit the product distribution is therefore narrow with benzene and formaldehyde* or its transformed species like methanol (eq 7).

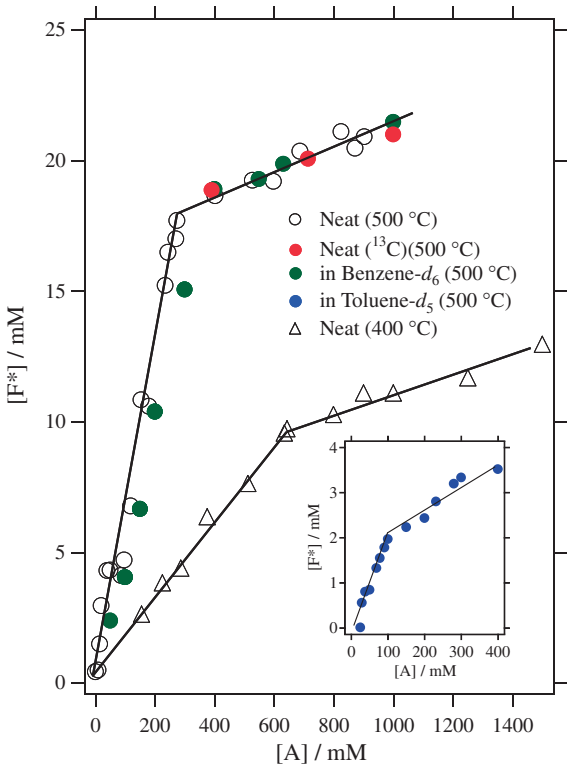

Figure 5. Relation between [F*] and [A] in supercritical anisole, anisole/1.0-M benzene-d_6 and anisole/1.0-M toluene-d_5 (inset) at 400 and 500 °C.

Table 1. Rate Constants, k_1 and k_2, Determined at 500 °C at High and Low Concentrations together with the Linear Parameters, α and β, in eqs 11 and 12

	concn Region	$10^3 k_1/s^{-1}$	$k_2/s^{-1}M^{-1}$	α^{HC}	β^{HC}	α^{LC}
Neat	HC	1.9 ± 0.2	0.12 ± 0.02	0.0040	17.0	
	LC	1.9 ± 0.2	0.12 ± 0.02			0.064
	1.0 mM	2.0 ± 0.3				
Benzene-d_6	HC	1.8 ± 0.3	0.11 ± 0.03	0.0035	17.5	
	LC	2.1 ± 0.3	0.12 ± 0.03			0.062
	1.0 mM	1.8 ± 0.4				
Toluene-d_5	HC	2.0 ± 0.4	0.40 ± 0.08	0.0056	1.41	
	LC	2.2 ± 0.4	0.70 ± 0.08			0.0189
	1.0 mM	1.8 ± 0.4				

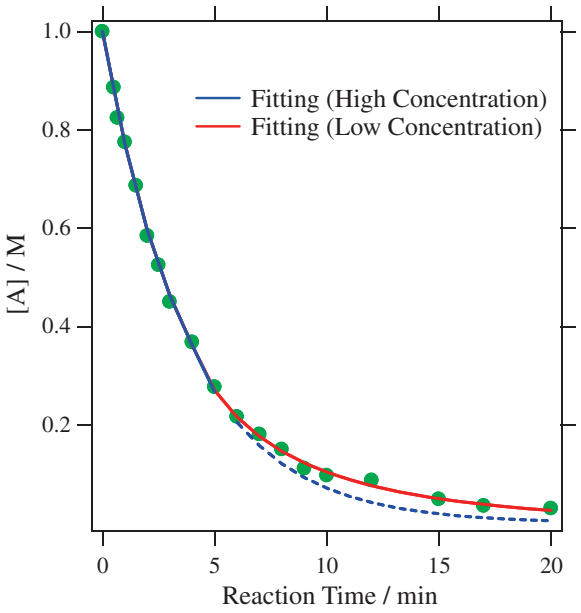

Figure 6. Time dependence of anisole concentration at 500 °C; the initial concentration is 1.0 M. Equations 14 and 15 are respectively fitted to the high-concentration (early-time) and the low-concentration (late-time) data; see the text.

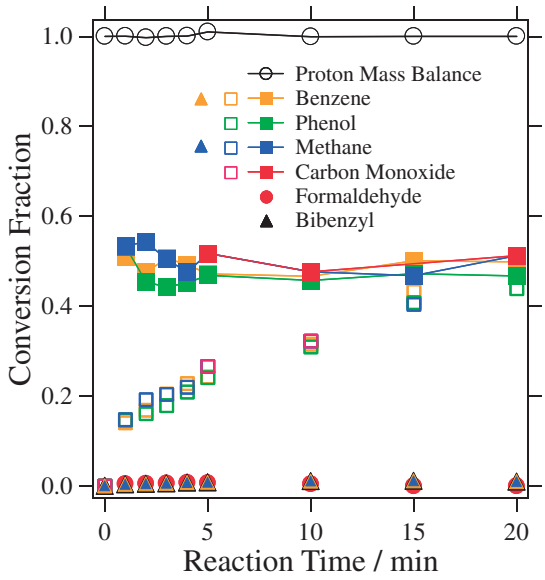

Figure 7. Time dependencies of conversion fractions f (closed squares) for the four major products and formaldehyde (closed circle) in the pyrolysis of anisole ($[A]_0 = 280$ mM) in supercritical toluene (1.0 M) at 500 °C; $f = -\Delta[\text{product}]/2\Delta[A]$. Open squares denote $[\text{product}]/[A]_0$. Solid triangles denote $[\text{product}]/[\text{toluene}]_0$.

Figure 6 shows how the initial depletion of anisole (A) at a high initial concentration (1.0 M) is expressed by eq 14 as long as [A] remains larger than the crossover concentration (>ca. 250 mM). When anisole is depleted below this point eq 14 cannot be used to reproduce the kinetic data; see the broken-curve in Figure 6. The long-time portion of the anisole depletion data are represented by eq 15 (red curve) but not by eq 14. The values of k_1 and k_2 thus determined are summarized in Table 1. The values obtained in different ways are in good agreement. Now we are ready to demonstrate the agreement of the rate constant k_1 between the HC and LC limits in a more direct manner. As compared in Table 1, the k_1 value thus calculated for neat anisole at the initial concentration of 1.0 M is in excellent agreement with that directly obtained through eq 19 in the LC region (1.0 mM). Thus the generality of the heterolytic reaction mechanism is confirmed by the self-consistency of the kinetics. No new channel is opened in the LC region.

One subject remaining to be scrutinized is the effect of supercritical solvent or carrier gases on the reaction pathways and the product distribution. The effect of toluene was discussed in terms of the radical mechanism in the previous works.[6,9] All of our main products, benzene, phenol, and methane except for carbon monoxide were also reported in Ref. 9, whereas only phenol and methane were identified in Ref. 6. We reinvestigated the effect of toluene in the anisole (0.001–1.0 M) and toluene (1.0 M) mixtures. Figure 7 displays the ^{1}H mass balance with respect to the anisole reaction and the time evolution of all of the species involved in the pyrolysis of ^{13}C-*labeled* anisole ($H_3{}^{13}CO{}^{12}C_6H_5$; 280 mM, double the crossover concentration in the HC region) in *normal* toluene ($H_3{}^{12}C{}^{12}C_6H_5$; 1.0 M) at 500 °C. As shown, in fact, there are the four main products as well as formaldehyde*. They are all in almost equal amounts at any time as in the case of neat anisole (1 M) shown in Figure 3. The characteristic profiles of Figure 7 are quite common to those of Figure 3. Although the minor products, toluene (eq 6) and methanol (eq 7), are also observed, respectively, at ≈1 and ≈2 mM (similar to the concentration of formaldehyde*) in toluene, they are omitted to avoid the overlapping in the plots. The minor products are generated less than those in the neat reaction because of the larger value of k_2. In addition to ^{13}C-labeled methane ($H_4{}^{13}C$; doublet ^{1}H signal as seen in Figure 1) that comes from the enriched solute anisole, normal methane ($H_4{}^{12}C$; singlet ^{1}H signal) and bibenzyl were observed in almost equal amounts. They are thought to be formed by the following overall reaction of supercritical solvent toluene:

$$3H_3{}^{12}C{}^{12}C_6H_5 \rightarrow H_4{}^{12}C + {}^{12}C_6H_6 + {}^{12}C_6H_5{}^{12}CH_2H_2{}^{12}C{}^{12}C_6H_5 \quad (20)$$

In any species here is no insertion of ^{13}C isotope. The identification of these solvent products is also ascertained by using the site-selectively deuterated anisole and toluene. The evolution of bibenzyl seems to be almost saturated when anisole is consumed, which indicates the influence of anisole on the solvent side-reaction. The reaction mechanism of this solvent side-reaction is unknown.

When toluene is added in excess [F*] is lower than that in benzene. As observed thus the toluene system can give the main products at a lower anisole concentration. These are reflected in the quantitative values of k_1 and k_2 summarized in Table 1. The agreement of the k_1 values in the HC and LC limits are excellent. The k_1 value obtained here for anisole at high and low concentrations in toluene is in harmony with the literature (interpolated) value, 1.9×10^{-3} s^{-1}, reported for anisole at low concentrations (0.2–0.8 mM) in toluene by Paul

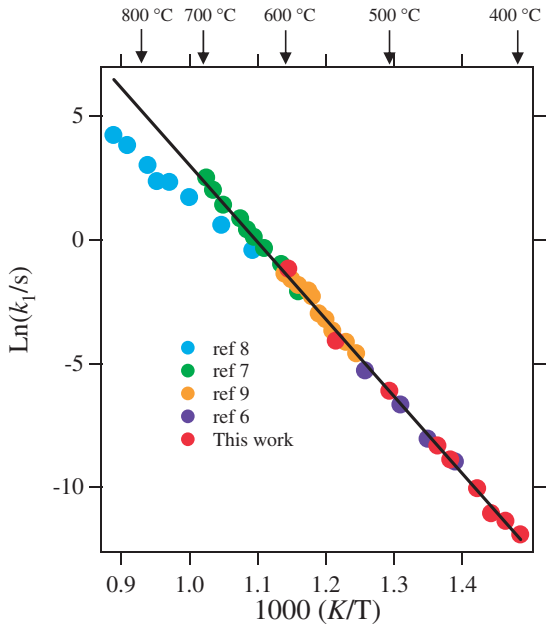

Figure 8. Arrhenius plots of rate constants, k_1, for the unimolecular decomposition of anisole; for the k_1 definition see the text. The experimental data shown in Refs. 6, 7, and 9 were graphically read. Their anisole concentrations were more or less than 1.0 mM.

and Back;[6] recall that their products are quite similar to ours as mentioned above. Even when the alien gas is added in excess the reaction mechanism does *not change* from the heterolytic to the homolytic.

One of the most important remaining problems is the effect of temperature on the rate constant of k_1. The Arrhenius plot of the unimolecular process is shown in Figure 8 for comparison. It is clearly shown that all of the rate constants determined by different groups at different temperatures are all lying in the single straight line within experimental uncertainties over the wide range of temperature. The general form of the Arrhenius plot for the pyrolysis of neat anisole is expressed by

$$k_1 = A \exp(-E_a/RT) \quad (21)$$

Here the frequency factor $A = (6.8 \pm 0.5) \times 10^{14}\,s^{-1}$ and the activation energy E_a is $259 \pm 8\,kJ\,mol^{-1}$; R is the gas constant and T the temperature. The E_a value obtained from the wide temperature range is in reasonable agreement with those reported in the narrower temperature range.[6,7,9] As seen in Figure 8, however, one paper[8] reports a considerably smaller E_a value.[25] Thus the anisole pyrolysis reaction discussed here is essentially the same as that so far studied.[5–12] The reaction mechanism proposed here is heterolytic for the reason discussed above.

Conclusion

We have focused on the combined application of site-selective labeling and high-resolution NMR spectroscopy in the gas and liquid phases in order to establish the reaction pathways and mechanism of the pyrolysis of the asymmetric ether, anisole. The reaction is composed of the elementary steps expressed by eqs 1 and 2. It is confirmed by the comprehensive product analysis that the four major products, benzene, phenol, methane, and carbon monoxide as well as the reactive intermediate formaldehyde* given by these elementary steps. In addition to the main reaction pathways, the side-reaction pathways leading to the formation of toluene and methanol by the consumption of the reactive intermediate formaldehyde* are disclosed. The conclusion drawn here on the CO generation pathway and the phenyl ring retention disfavors the prevailing mechanism that CO is generated through the phenoxy radical.[5–12] The pyrolysis studied is not homolytic but heterolytic over wide enough ranges of concentrations and temperatures. The self-consistency of the kinetics has been firmly confirmed. Further study on the pyrolysis of the methoxy ether, anisole is in progress by using multinuclear NMR spectroscopy and site-selectively deuterated anisole isotopes, in order to obtain more direct evidence for the proton-transfer mechanism. It is suggested that in situ vibrational spectroscopic study could provide us with more detailed quantum states involved in the pyrolysis. What are found here would make a contribution to advances in science and technology for non-catalytic thermal cracking of fuel-related compounds at high temperatures.

This work is supported by the Grants-in-Aid for Scientific Research (Nos. 18350004 and 21300111) from the Japan Society for the Promotion of Science and by the Grants-in-Aid for Scientific Research on Priority Areas (Nos. 15076205 and 20038034), the Grant-in-Aid for Scientific Research on Innovative Areas (No. 20118002), and the Next-Generation Integrated Nanoscience Simulation Software Project from the MEXT. N. M. is also grateful to the CREST project from Japan Science and Technology Agency (JST) and to the grant from the Association for the Progress of New Chemistry, the grant from the Suntory Institute for Bioorganic Research, and the Supercomputer Laboratory of Institute for Chemical Research, Kyoto University. M. N. and Y. T. acknowledge the donation of The Water Chemistry Energy Laboratory (AGC) from Asahi Glass Co., Ltd.

References

1 Y. Tsujino, C. Wakai, N. Matubayasi, M. Nakahara, *Chem. Lett.* **2006**, *35*, 1334.
2 Y. Nagai, S. Morooka, N. Matubayasi, M. Nakahara, *J. Phys. Chem. A* **2004**, *108*, 11635.
3 Y. Nagai, N. Matubayasi, M. Nakahara, *J. Phys. Chem. A* **2005**, *109*, 3550, and papers cited therein.
4 Y. Nagai, N. Matubayasi, M. Nakahara, *J. Phys. Chem. A* **2005**, *109*, 3558.
5 A. G. Harrison, L. R. Honnen, H. J. Dauben, Jr., F. P. Lossing, *J. Am. Chem. Soc.* **1960**, *82*, 5593.
6 S. Paul, M. H. Back, *Can. J. Chem.* **1975**, *53*, 3330.
7 J. C. Mackie, K. R. Doolan, P. F. Nelson, *J. Phys. Chem.* **1989**, *93*, 664.
8 M. M. Suryan, S. A. Kafafi, S. E. Stein, *J. Am. Chem. Soc.* **1989**, *111*, 1423.
9 I. W. C. E. Arends, R. Louw, P. Mulder, *J. Phys. Chem.* **1993**, *97*, 7914.
10 M. Pecullan, K. Brezinsky, I. Glassman, *J. Phys. Chem. A* **1997**, *101*, 3305.

11 V. V. Platonov, V. A. Proskuryakov, S. V. Ryl'tsova, Yu. N. Popova, *Russ. J. Appl. Chem.* **2001**, *74*, 1047.

12 A. V. Friderichsen, E.-J. Shin, R. J. Evans, M. R. Nimlos, D. C. Dayton, G. B. Ellison, *Fuel* **2001**, *80*, 1747.

13 C. N. Hinshelwood, P. J. Askey, *Proc. R. Soc. London, Ser. A* **1927**, *115*, 215.

14 M. B. Smith, J. March, *Advanced Organic Chemistry: Reaction, Mechanism, and Structure*, 5th ed., John Wiley & Sons, New York, **2001**, p. 477.

15 S. Morooka, N. Matubayasi, M. Nakahara, *J. Phys. Chem. A* **2007**, *111*, 2697.

16 The critical temperature and density of anisole were determined to be 393 ± 1 °C and 0.32 ± 0.03 g cm^{-3} (3.0 ± 0.3 M), respectively. The critical temperatures for benzene and toluene are 289 and 319 °C, respectively. Thus all of the anisole reactions studied here occurred under supercritical conditions.

17 High-velocity collisions can excite C–H vibrations composed of the very light H atoms. The following kinetic data led us to assume the vibronically excited formaldehyde* as a reactive intermediate in eq 1 that is to cross over dissociative curves onto which the fragmentation reaction manifold is projected. The reaction rate of anisole depletion at 1.0 M was not affected by addition of a formaldehyde generator, 1,3,5-trioxane that can be completely decomposed and decayed into ground-state monomers at 200–250 °C. The initial depletion rate constants with and without ground-state formaldehyde at 100 mM in excess at 500 °C are $(1.9 \pm 0.1) \times 10^{-3}$ and $(1.6 \pm 0.3) \times 10^{-3}$ s^{-1}, respectively. These values are almost identical.

18 For the case of the asymmetric ether (anisole) the reaction pathways are fully separated. For the case of the symmetric ether, dimethyl ether, however, the products as well as the pathways are not completely distinguished. Compare the fragmentation products of anisole and dimethyl ether,[4] and we have the following correspondence: benzene ⇔ methane, phenol ⇔ methanol, toluene ⇔ ethane. Thus the products overlap significantly in the case of dimethyl ether whose mechanism has been discussed in the same way based on the heterolytic mechanism. Thus ethane is not formed from the combination of methyl radicals.

19 The CO conversion fraction is always larger than that for phenol because of the contributions from the side-reactions, eqs 6 and 7 as well as eq 2; see Figure 4. The corresponding mass balance is: [carbon monoxide](overall) = [phenol](eq 2) + [toluene](eq 6) + [methanol](eq 7).

20 It is important to show no appearance of products related to the homolysis-originated methyl radical, that is the counterpart of phenoxy radical. The ^{13}C, ^{2}H, and ^{1}H NMR spectroscopic study on the toluene-d_5 system clearly indicates that the minor product, bibenzyl is generated not from anisole but from the high-concentration supercritical solvation shell itself,[21] contrary to the phenoxy-radical mechanism.[6,9] Furthermore, when benzene-d_6 or toluene-d_5 is added to anisole to change the molecular environment no propagation products of methyl and hydrogen radicals assumed in the literature are detected. In other words, no ^{1}H-methyl-substituted derivatives of the deuterated solvents are detected.

21 Y. Yoshida, N. Matubayasi, M. Nakahara, *J. Chem. Phys.* **2007**, *127*, 174509.

22 Some complex or cluster formation can be induced by the attractive polarization effect on the phenyl π-electrons provided by the strong dipole of F* and/or by the repulsion effect by the blocking cage molecules.

23 It is interesting to compare the proton-transferred reaction mechanism (heterolytic) proposed here and the traditional unimolecular reaction mechanism (homolytic) given by the Lindemann–Hinshelwood theory because a work[8] heavily relies upon the RRKM theory:[24] $A + A \rightleftarrows A + A^*$ and $A^* \rightarrow P$
for which the rate constants for the activation and the deactivation of the activated species A* are defined, respectively, by k_{+a} and k_{-a}, and that for the transformation of A* into the product P is denote by k_b. The steady-state approximation leads us to:
$d[P]/dt = k_b[A^*] = k_a k_b[A]^2/(k_b + k_{-a}[A])$,
which is reduced to:
$d[P]/dt = (k_a k_b/k_{-a})\,[A]$
for the high-pressure condition, $k_{-a}[A^*][A] \gg k_b[A^*]$, and
$d[P]/dt = k_a\,[A]^2$
for the low-pressure condition, $k_{-a}[A^*][A] \ll k_b[A^*]$.
Common to the two mechanisms, the reaction order is controlled by the magnitude of the concentration [A], leading to the high- and low-pressure (concentration) limits. The essential difference, however, exists in the reaction order in the low-concentration limit. The present and the Lindemann–Hinshelwood mechanisms respectively give the 1st- and 2nd-order reactions; see eq 19 and the derivation for the rate law. Also in the high-concentration limit, our expression by eq 13 or 14 (solution) is more accurate and useful for the concentration dependence over a wide concentration range including the high.

24 J. I. Steinfeld, J. S. Francisco, W. L. Hase, *Chemical Kinetics and Dynamics*, 2nd ed., Prentice Hall, New Jersey, **1999**, Chap. 11.

25 Although the rate constants experimentally determined[8] at temperatures higher than 600 °C are smaller than those provided by the Arrhenius line, those extrapolated with the help of the RRKM theory to the temperature range of 450–550 °C are said to be in good agreement in Ref. 9 (Figure 3).